Level structure of ^{140}Nd

E. Gülmez,* H. Li, and J. A. Cizewski†
A.W. Wright Nuclear Structure Laboratory, Yale University, New Haven, Connecticut 06511
(Received 9 April 1987)

The structure of ^{140}Nd has been studied via the ^{126}Te(^{18}O,4n)^{140}Nd and ^{128}Te(^{16}O,4n)^{140}Nd reactions at beam energies from 64 to 76 MeV and 72 to 76 MeV, respectively. In beam γ-ray spectroscopy techniques, including γ-ray excitation functions, γ-γ coincidences, and γ-ray angular distribution measurements, were used to construct a level scheme up to $J=17$ at an excitation energy of 6411 keV. Definite parity assignments were made up to the 11^+ state. Two-particle configurations were calculated with a shell model and a modified surface delta interaction.

I. INTRODUCTION

The nuclei in the neutron deficient region below $Z<64$, $N<82$ have been predicted[1] to be highly deformed with $\beta \geq 0.3$ for the very neutron deficient nuclei, such as ^{123}Ce, ^{126}Pr, ^{130}Nd, and ^{135}Pm. ^{135}Pm is the most notable, because it is much closer to the valley of stability and can be reached easily via (heavy-ion, xn) reactions. Recent studies of light cerium isotopes[2–7] show that they are deformed and can be explained within the triaxial-rotor plus particle model.[7] The deformations that have been extracted from the experimental level structures are reproduced by the calculations performed by Leander and Möller.[1] Light neodymium isotopes, although less extensively studied, show the same behavior.[8–11] Also, the most recent data[11] on the neutron deficient Pm nuclei clearly exhibit a deformed structure.

As one goes towards the $N=82$ shell closure the rotational structure begins to disappear and spherical single particle configurations dominate the low-lying level structure of the nuclei with $N \leq 82$; ^{138}Ce and ^{140}Nd are very good examples of this type of structure. For instance 7^- isomers, at 2128 and 2222 keV, respectively, in both nuclei can be explained[12,13] with a $(\nu h_{11/2}^{-1} \nu d_{3/2}^{-1})_{7^-}$ configuration and 10^+ isomers at 3538 and 3622 keV, respectively, with a $(\nu h_{11/2}^{-2})_{10^+}$ configuration.[13]

To further establish the onset of deformation at high angular momentum in the $Z<64$, $N<82$ nuclei we have initiated a program to study the high spin structure of the $N=80$ isotones ^{141}Pm and ^{140}Nd. Although earlier studies of ^{140}Nd with heavy ions had established the γ-ray deexcitation scheme up to 6408 keV, these results[13] did not provide definite spin-parity assignments for higher angular momentum states. In the present paper we report on our measurements of the γ-ray deexcitation scheme of ^{140}Nd populated with ^{18,16}O beams where the ^{18}O beam was chosen to complement our concurrent study[14] of ^{141}Pm with a ^{19}F beam. Preliminary results of our ^{140}Nd measurements have been presented.[15,16]

II. EXPERIMENTAL PROCEDURE

The nucleus ^{140}Nd was populated with a heavy-ion fusion evaporation reaction using ^{16,18}O beams from the Yale MP tandem Van de Graaff accelerator. Isotopically enriched ^{126,128}Te targets (≈ 1 mg/cm^2) were evaporated onto Au and Bi foils of ≈ 10 mg/cm^2. In the experiment the beam was stopped in the target assembly by using a very thick natural lead foil which was placed immediately after the target backing.

The γ-ray deexcitation of the nuclei produced in these interactions was studied by standard γ-ray spectroscopy techniques. The γ rays were detected with three germanium detectors: an n-type high purity germanium coaxial "gamma-x" detector with an efficiency of $\approx 25\%$ and a nominal total active area of 85 cm^2, a Ge(Li) detector with an efficiency of 20% and a nominal active volume of 100 cm^3, and a 12% Ge(Li) detector with a nominal active volume of 65 cm^3. [All efficiences are relative to a 7.6×7.6 cm^2 NaI(Tl) scintillator.] Typical energy resolutions of these detectors for our measurements were 2.75, 2.25, and 2.75 keV full width at half maximum (FWHM), respectively, at 1332 keV.

Gamma-ray excitation functions were measured for a beam energy of 64–76 MeV for ^{18}O and 72–76 MeV for ^{16}O in 2 MeV steps. Gamma-ray yields were normalized using Coulomb excitation lines of the Te target in each spectrum. Gamma-gamma coincidence measurements were made with the ^{126}Te target. The ^{128}Te target was used for angular distribution measurements.

The optimum beam energies for populating the 4n (^{140}Nd) channel were determined to be 72 and 76 MeV for the ^{18}O and ^{16}O beams, respectively, by examining several strong γ-ray transitions in ^{140}Nd, such as the three transitions below the 7^- isomer and the one feeding this isomer. The large difference between these two optimum energies for the 4n (^{140}Nd) channel was because the ^{128}Te target had alloyed with the Bi backing.

In our γ-γ coincidence measurements three types of coincidence events were recorded utilizing the three Ge detectors placed at 90°, 0°, and −90° with respect to beam line. The electronic time resolution obtained in

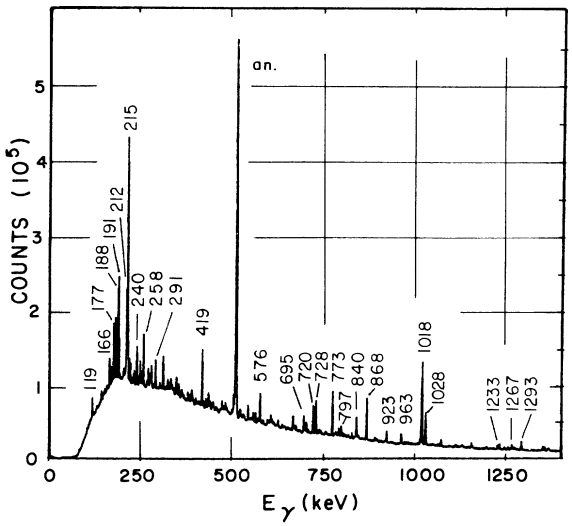

FIG. 1. Spectrum of coincident gamma rays observed in the 20% Ge(Li) detector for the $^{18}O + {}^{126}Te$ reaction.

this experiment was ≈ 20 ns. A total of 41 million raw events was recorded event by event on magnetic tapes for subsequent off-line analysis. These data were analyzed first by sorting into a 2800×2800 $E1 \times E2$ matrix and then adding the corresponding rows and columns for a specific gate, thus doubling the statistics. Figure 1 shows a spectrum taken with the 20% Ge(Li) detector of all prompt γ rays coincident between this and the gamma-x detector. Figure 2 shows several coincidence spectra gated by specific lines.

The angular distribution measurements were carried out with a ^{16}O beam energy of 76 MeV on the ^{128}Te target. Data were collected from 0° to 90°, with respect to the beam, in 15° increments. The data at different angles were normalized using the yields of the three isotropic transitions below the 0.6 ms 7^- isomer.[17] The accuracy in the normalization factors was better than 2%. Gamma-ray efficiencies of the system were determined by using ^{152}Eu and ^{133}Ba γ-ray sources. The peak areas as functions of angle were fitted with a fourth order truncated Legendre polynomial:

$$W(\theta) = A_0 + A_2 P_2(\cos\theta) + A_4 P_4(\cos\theta) \quad (1)$$

and corrected for the solid angle effects. Angular distribution coefficients and intensities of γ rays extracted are listed in Tables I and II.

In using the angular distribution coefficients to assign multipolarities to transitions we assumed that,[18] (a) pure $J \pm 2 \rightarrow J$ transitions have $A_2 > 0$, $A_4 < 0$, (b) $J \pm 1 \rightarrow J$ transitions have $A_4 \geq 0$ for all mixing ratios, (c) $J \rightarrow J$ transitions have $A_4 \leq 0$ for all mixing ratios, and that the transitions are stretched, i.e., only $J+2 \rightarrow J$, $J+1 \rightarrow J$, or $J \rightarrow J$, given the previously established[12] J^π values. With these assumptions we can extract attenuation coefficients α_2 for the nuclear alignment; we find $\alpha_2 > 0.5$ for all transitions.

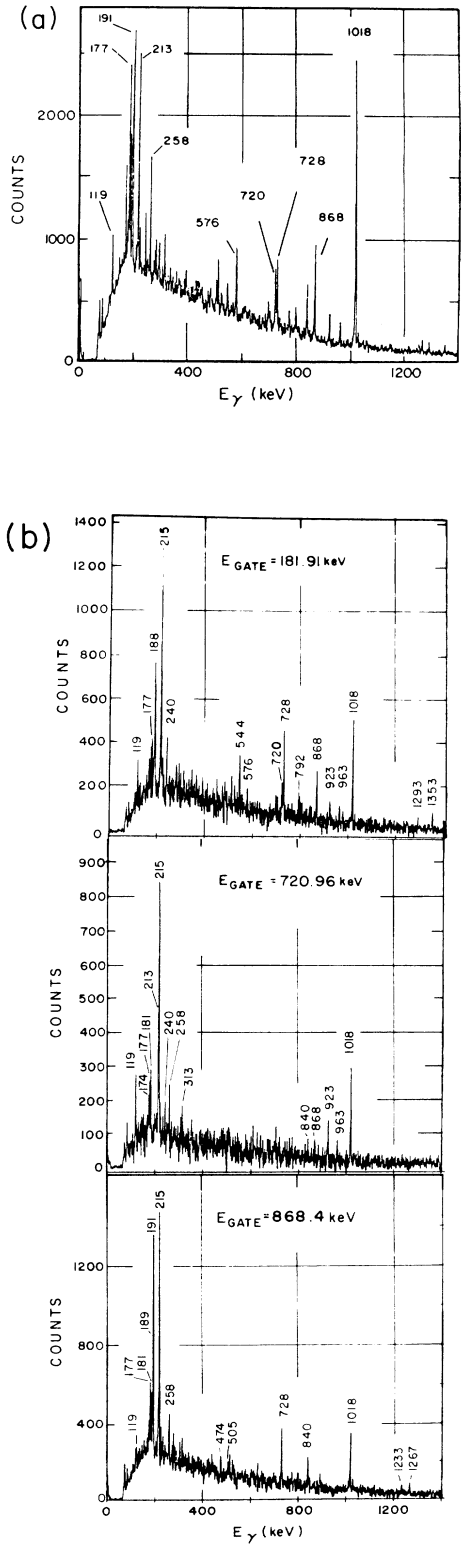

FIG. 2. (a) Compton subtracted γ-γ coincidence spectrum obtained when gating on the 215 keV transition in ^{140}Nd. (b) Compton subtracted γ-γ coincidence spectra obtained when gating on the 181, 868, and 721 keV transitions in ^{140}Nd.

III. LEVEL SPECTRUM

Combining the results of the γ-γ coincidence, angular distribution, and excitation function measurements, the deexcitation scheme in Fig. 3 was deduced. The half-lives of the isomers and the multipolarities of the transitions below the 7^- isomer were taken from Ref. 17.

For the most part our level spectrum agrees with that reported by Ludziejewski and Arnold[12] and Merdinger.[13] Below the 3455 keV 9^- level our spectrum is identical to that previously reported by Ludziejewski and Arnold, with little differences in the energies of the transitions. We determined the parity of the 2366 keV level to be positive, based on the multipolarity that we extracted from angular distribution measurements for the 564 keV transition which depopulates it. Although the 90 keV transition was not seen strongly in the 474 and 695 keV gates, we placed it because of the prompt coincidence between the 474, 695, 1028, and 773 keV transitions. Because the (α,xn) reaction was used to populate ^{140}Nd in Ref. 12, above the 3455 keV level there is essentially no similarity between the spectrum of Ref. 12 and that shown in Fig. 3.

There are several differences between our deexcitation scheme and that reported by Merdinger[13] from the ^{128}Te(^{16}O, 4nγ) reaction. In Ref. 13 there are two cascades feeding the 3455 keV 9^- level. We also populate these two cascades but with some changes in the order of transitions in the cascades. In the cascade of the 213, 119, 720, 923, 181, and 240 keV transitions, we placed the 119 keV transition above the 923 keV transition. The intensity of this γ ray and the relative strength of this line in the 213, 720, and 923 keV prompt gates [Fig. 2(b)] do not allow us to place it directly above the 213 keV transition; rather it fits very well just above the 923 keV transition. The spin parity of the 3668.9 keV level was assigned 10^- by Merdinger.[13] However, in our spectra the 213 keV line belongs to a triplet, and therefore we do not make a definite multipolarity assignment to this transition. However, our measurement is not inconsistent with the 10^- assignment to the 3668.9 keV level. We also have a secondary cascade feeding the 4389.9 keV level, namely the 963 and 174 keV transitions. We see a new transition feeding the 5614.6 keV level.

In the second main cascade, the 505, 258, 212, 728, 188, 191, and 868 keV γ rays, the γ-γ coincidence gates for the 868 and 188 keV lines, and the intensity of the 191 keV line indicated the placement of the 191 keV line above the 868 keV and below the 188 keV transitions [Fig. 2(b)], inverting the order reported in the previous work.[13] In this cascade we have made definite spin-parity assignments up to the 4324.0 keV level. (We are limited to tentative assignments above this because the 188 and 191 keV lines are doublets in our spectra.) The earlier work assigned definite spin parity values only up to the 3455 keV level. Only tentative spin values have been assigned to levels above the 5432 keV level because we were unable to assign a multipolarity to the 212 keV line, a weak component of a triplet of lines in our spectra. In addition to the two intense cascades reported previously,[13] we have placed several weaker transitions in our deexcitation scheme shown in Fig. 3.

We have determined the half-life of the 10^+ isomer at 3622.2 keV to be 25(8) ns, in agreement with the earlier results[13,19] of Merdinger and co-workers reported as 22 ns and 32(1) ns. Given our coarse time resolution we were unable to confirm the half-life of the reported[13] 0.25 ns 12^+ isomer at 4515.1 keV.

TABLE I. Results from angular distribution measurements of transitions in ^{140}Nd. The angular distribution coefficients were determined with Eq. (1). The results are further discussed in Ref. 16 where sample fits are presented.

E (keV)	A_2/A_0	A_4/A_0	δ
90.06(3)	−0.05(3)	−0.20(3)	
119.95(4)	−0.18(6)	−0.06(7)	
144.78(6)	−0.31(9)	0.01(11)	
166.57(4)	−0.05(4)	−0.08(5)	
174.84(6)	−0.26(8)	0.19(12)	$-5^{+4.3}_{-\infty}$
177.38(4)	−0.38(2)	−0.01(3)	$-0.4^{0.4}_{-0.3}$
181.91(4)	−0.24(2)	−0.04(3)	
188.95(4)	−0.25(2)	0.01(3)	$-5^{+1.5}_{-1.5}$
191.09(4)	−0.09(2)	−0.07(2)	
212.48(4)[a]	−0.19(3)	−0.12(4)	
215.28(3)	−0.41(1)	−0.01(1)	$-0.25^{+0.25}_{-0.10}$
240.56(5)	−0.35(5)	0.02(6)	
258.53(4)	−0.26(3)	0.00(4)	
291.77(5)	−0.42(5)	0.02(6)	$-0.8^{+0.5}_{-\infty}$
419.49(5)	−0.01(1)	0.02(1)	
439.85(6)	−0.59(3)	0.30(3)	
474.01(7)	−0.14(7)	−0.05(10)	
483.86(7)	0.70(9)	−0.25(11)	
505.27(8)	−0.29(9)	−0.27(12)	
544.44(9)	−0.29(8)	0.04(11)	$-0.15^{+0.15}_{-1.35}$
564.42(8)	0.33(6)	−0.12(8)	
576.17(8)	−0.80(4)	0.21(5)	$-1.9^{+1.1}_{-2.1}$
695.51(9)	−0.10(4)	0.05(4)	
720.96(9)	−0.27(2)	0.08(2)	$-4^{+1}_{-\infty}$
728.60(8)	−0.25(2)	0.06(2)	$-3^{+1.6}_{-\infty}$
773.85(9)	0.01(1)	0.02(1)	
797.8(1)	−0.37(4)	0.02(5)	$-0.3^{+0.3}_{-0.5}$
840.4(1)	0.25(2)	−0.02(2)	$-0.25^{+0.25}_{-0.20}$
868.4(1)	0.18(1)	−0.06(1)	
923.3(1)	0.30(3)	−0.10(3)	
963.0(1)	0.17(4)	−0.16(4)	
1018.2(1)	−0.86(1)	0.19(1)	$-1.7^{+0.5}_{-\infty}$
1028.8(1)	0.01(1)	0.02(1)	
1233.5(2)	0.29(4)	−0.06(5)	
1267.5(2)	0.16(6)	−0.06(8)	
1293.6(2)	−0.70(4)	0.06(5)	$-0.4^{+0.4}_{-0.4}$

[a]Composite line.

IV. DISCUSSION

The ^{140}Nd nucleus has ten protons outside of the $Z=50$ core or four holes in the $Z=64$ core and two holes in the $N=82$ core. With valence protons and neutrons, one would expect it to show vibrational excitations at low energies and particle or hole excitations as

the excitation energy increases.

To further understand the nature of the low-lying levels and isomers one can look at the Nd systematics (Fig. 4) and $N=80$ systematics (Fig. 5). As seen in Fig. 5, the excitation energies of the 7^- and 10^+ isomers do not change substantially below or above the $Z=64$ shell gap, hence indicating a similar structure for these states for the $N=80$ isotones. However, when we examine the Nd systematics in Fig. 4 the excitation energies of the 7^- and 10^+ isomers change dramatically. The g factor measurement of the 10^+ isomer[19] further supports the interpretation as a neutron configuration, because the measured value of $-0.191(12)$ is exactly the single particle estimate[20] for a neutron configuration. Therefore, we can conclude that the low-lying levels in ^{140}Nd, and in particular the two 7^- and 10^+ isomers at excitation energies of 2222 and 3622 keV, respectively, should be mostly two neutron hole excitations.

To gain a better understanding of the low-lying structure of ^{140}Nd, we have performed a spherical shell model calculation for two-particle configurations. The excitation energies of the two-particle configurations can be calculated simply by adding the single-particle energies and the residual interaction energy as follows:

$$E_J=\epsilon_{j_1}+\epsilon_{j_2}+\Delta E_j(j_1 j_2;j_1 j_2)\ , \tag{2}$$

TABLE II. γ-ray transitions placed in the deexcitation scheme of ^{140}Nd. (The energies quoted in the text are truncated to the nearest integer and the energies given in the level scheme of Fig. 3 are rounded to the nearest 0.1 keV.)

E (keV)	$J_i^\pi \rightarrow J_f^\pi$ [a]	I_γ [b]	Character
90.06(3)	$6_1^+ \rightarrow 5_1^-$		
119.95(4)	14(5432) $\rightarrow$ (13^-(5312))	207(11)	($E1$)
144.78(6)	$6_1^+ \rightarrow 7_1^-$	109(8)	
166.57(4)	$10_1^+ \rightarrow 9_1^-$	212(9)	($E1$)
174.84(6)	(14(5527)) $\rightarrow$ (13^-(5352))	77(6)	
177.38(4)	$8_1^- \rightarrow 7_2^-$	334(11)	$E2+M1$
181.91(4)	(15(5614)) $\rightarrow$ 14(5432)	327(11)	
188.95(4)	13(4704) $\rightarrow$ 12(4515)	452(15)	($E2+M1$)
191.09(4)	12(4515) $\rightarrow$ 11_1^-(4324)	542(16)	($\Delta J=1$)
212.3(5)[c]	(15(5645)) $\rightarrow$ 14(5432)	250(50)	
213.3(5)[c]	(10_1^-) $\rightarrow$ 9_1^-	350(50)	
215.28(3)	$9_1^- \rightarrow 8_1^-$	1072(26)	$E2+M1$
240.56(5)	(16(5855)) $\rightarrow$ (15(5614))	149(7)	
258.53(4)	(16(5903)) $\rightarrow$ (15(5645))	231(9)	
291.77(5)	$11_1^- \rightarrow 10_2^-$	137(7)	
419.49(5)	$7_1^- \rightarrow 4_1^+$	1994(46)	$E3$[d]
439.85(6)	6411 $\rightarrow$ (15(5971))	331(12)	
474.01(7)	$5_1^- \rightarrow 4_1^+$	96(6)	$E1$[d]
483.86(7)	12(4515) $\rightarrow$ 10_2^-(4031)	85(6)	
505.27(8)	(17(6408)) $\rightarrow$ (16(5903))	72(6)	
544.44(9)	(16(6159)) $\rightarrow$ (15(5614))	103(6)	
564.42(8)	$6_1^+ \rightarrow 4_1^+$	109(6)	$E2$
576.17(8)	$10_2^- \rightarrow 9_1^-$	200(9)	$E2+M1$
695.51(9)	$7_2^- \rightarrow 6_1^+$	233(10)	($E1$)
720.96(9)	(11_2^-(4389)) $\rightarrow$ (10_1^-(3668))	350(11)	$E2+M1$
728.60(8)	14(5432) $\rightarrow$ 13(4704)	414(13)	$E2+M1$
773.85(9)	$2_1^+ \rightarrow 0_1^+$	2456(56)	$E2$[d]
797.8(1)	(13^-(5312)) $\rightarrow$ 13(4704)	127(6)	
840.4(1)	$7_2^- \rightarrow 7_1^-$	447(14)	$E2+M1$
868.4(1)	$11_1^- \rightarrow 9_1^-$	954(24)	$E2$
923.3(1)	(13^-(5312)) $\rightarrow$ (11_2^-(4389))	263(9)	$E2$
963.0(1)	(13^-(5352)) $\rightarrow$ (11_2^-(4389))	229(10)	$E2$
1018.2(1)	$8_1^- \rightarrow 7_1^-$	1000(28)	$E2+M1$
1028.8(1)	$4_1^+ \rightarrow 2_1^+$	2425(56)	$E2$[d]
1233.5(2)	$9_1^- \rightarrow 7_1^-$	154(7)	$E2$
1267.5(2)	(15(5971)) $\rightarrow$ 13(4704)	119(5)	$E2$
1293.6(2)	$11_1^+ \rightarrow 10_1^+$	178(8)	$E2+M1$

[a]Spin parity of the initial and final levels as assigned in the level scheme shown in Fig. 3.
[b]Relative γ-ray transition intensities normalized to the 1018 keV γ-ray transition intensity. Errors on the last digits are in parentheses.
[c]Energies and intensities determined from the γ-γ coincidence gates.
[d]Multipolarities are taken from Refs. 12 and 13.

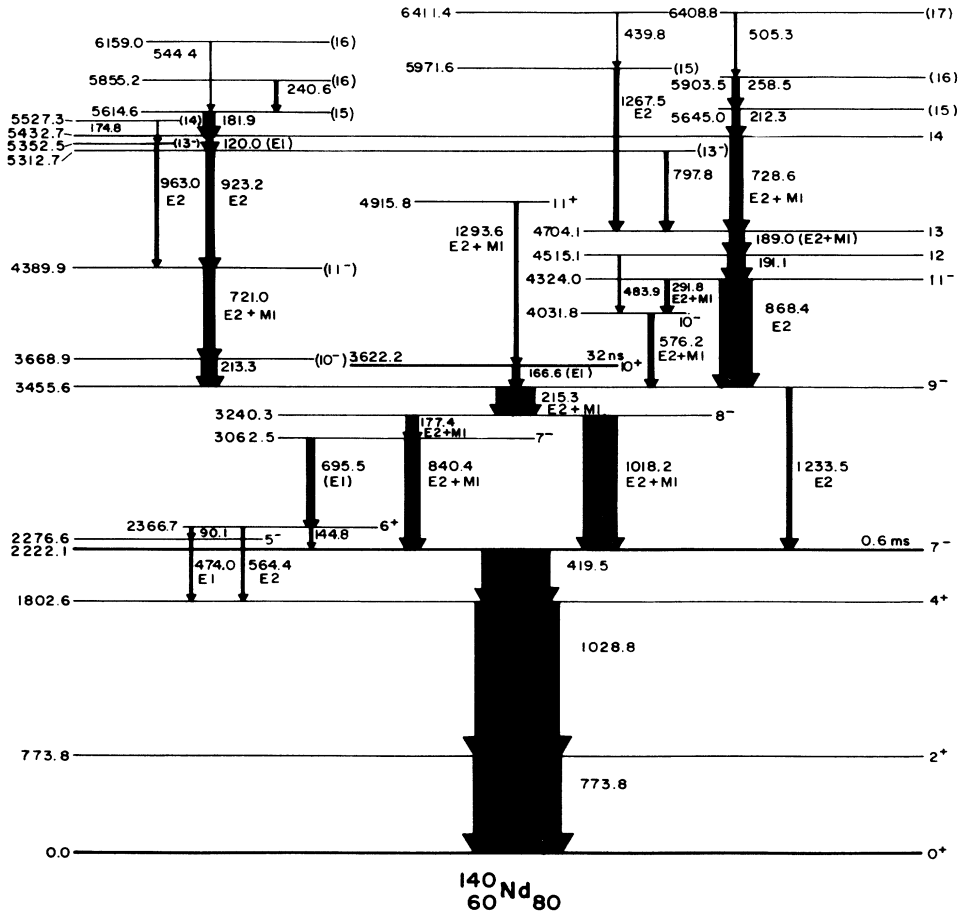

FIG. 3. The deexcitation scheme of ^{140}Nd obtained from the ^{126}Te(^{18}O,4nγ) reaction. See text for further discussion of spin, parity, and isomer assignments.

where the ϵ_j's are the single-particle energies for the orbitals involved, and ΔE_J is the residual interaction energy shift.

In our calculations, a modified surface delta interaction[21] (MSDI) was used which is slightly different from the simple δ interaction used in the previous studies[12] of shell model configurations in ^{140}Nd in that the δ interaction is modified under the assumption of only a surface interaction between nucleons. An isospin dependent constant term is added to the δ-function residual interaction in order to obtain a better fit. The final form of the residual interaction becomes

$$V_{ij}=4\pi A_T\delta(r_i-R)\delta(r_j-R)\delta(\Omega_{ij})+B_T\ , \tag{3}$$

where A_T is the interaction strength, B_T is the constant isospin term, R is the radius of the nucleus, and Ω_{ij} is the solid angle between r_i and r_j, the position vectors of each particle. The two parameters, A_T and B_T, depend on isospin T and are adjusted by equating the energies of two excited states with fairly well-established configurations, such as the 7^- and 10^+ isomers, to the calculated values.

We shall limit ourselves to a configuration space for neutrons: $3s_{1/2}$, $2d_{3/2}$, $2d_{5/2}$, $1g_{7/2}$, and $1h_{11/2}$; and for protons: $2d_{5/2}$, $1g_{7/2}$, and $1h_{11/2}$. In this basis space the only allowed configurations for the 7^- and 10^+ isomers will be $(\nu h_{11/2}^{-1}\nu d_{3/2}^{-1})_{7^-}$ and $(\nu h_{11/2}^{-2})_{10^+}$, respectively. As mentioned above, from these excited states we can determine the interaction strength $A_{T=1}$ and the isospin dependent constant term $B_{T=1}$. In principle, these parameters determined from pure neutron configurations should be valid for proton configurations. However, since we are not carrying out a general shell model fit, the interaction strength is expected to be different from the pure neutron configuration because of the Coulomb interaction. Hence, using the same B_1 and assuming that the ground state has a $(\pi d_{5/2}^2)_{0^+}$ configuration, we can determine the effective interaction strength A_1 for protons. The values of these parameters are $B_1=0.464$ MeV; $A_1R_0=0.575$ MeV for neutrons, and $A_1R_0=0.861$ MeV for protons. (R_0 is a constant coming from the radial parts of the wave functions.[20])

The single-particle energies can be determined from

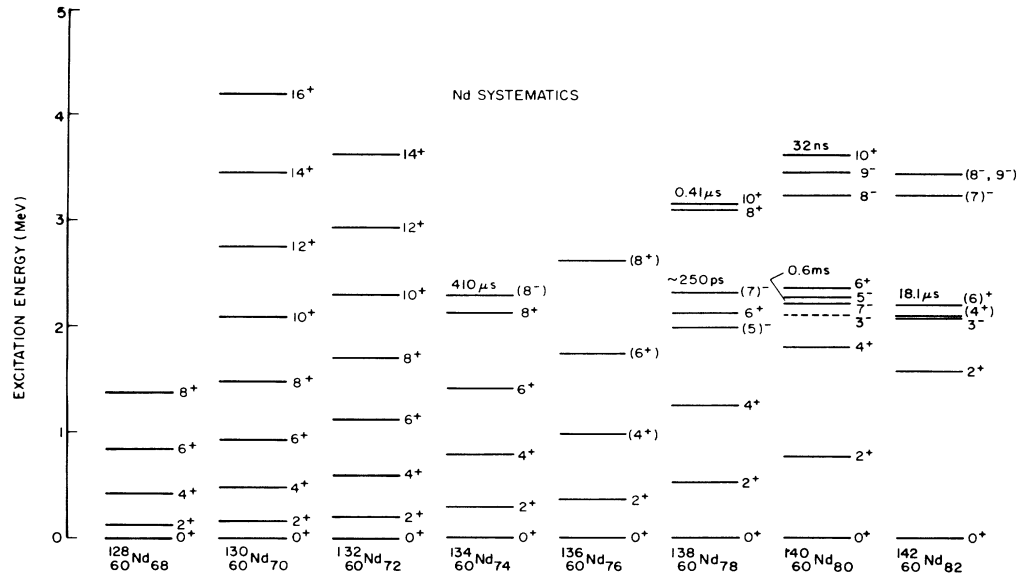

FIG. 4. The energy systematics of even-mass Nd nuclei (data taken from Refs. 17 and 25–28).

the adjacent odd-mass nuclei. The neutron single-particle energies relative to the ground state of ^{142}Nd are determined from the single-hole excitations in ^{141}Nd populated via the (p,d) reaction[22] on ^{142}Nd. For the protons, unfortunately, no single-particle transfer data are available. Therefore, we assumed the low-lying excitations[23] in ^{139}Pr to be single-particle excitations, which is justified because the first few excited states in neighboring odd-proton nuclei are known to be single-particle excitations from transfer reaction measurements (e.g., Ref. 24). The single-particle energies used in our calculations are summarized in Table III.

The results of our calculations are given in Fig. 6, where we also compare our data with previous results. The first 2^+ energy calculated for any configuration is much higher than the experimental value, indicating that the 2_1^+ state is a collective excitation. On the other hand, the calculated 4^+ energies are closer to the experi-

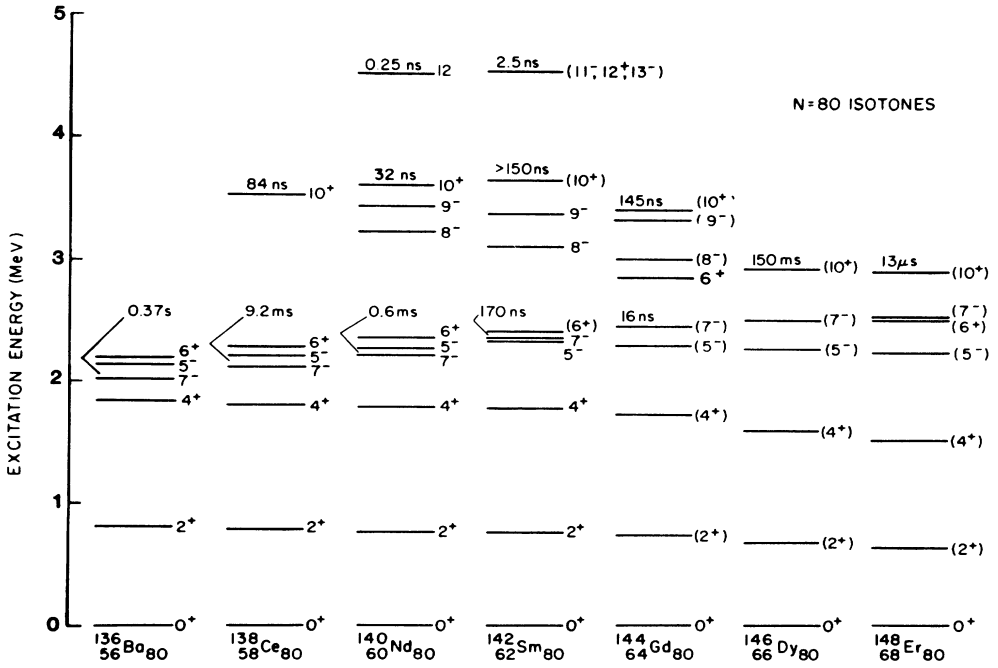

FIG. 5. The energy systematics of even-mass $N=80$ isotones (data taken from Refs. 26–30).

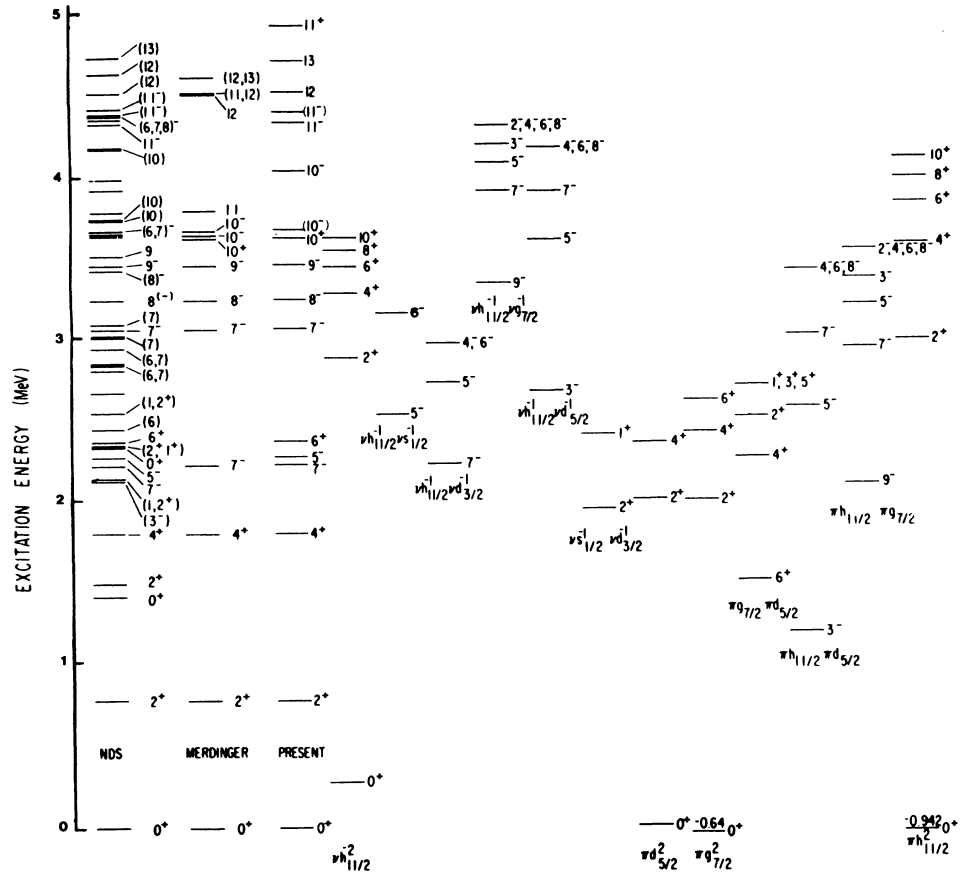

FIG. 6. Results of the shell model calculations for two-particle configurations using a modified surface delta interaction of Ref. 21. The columns are as follows: tabulated energies from Nuclear Data Sheets (NDS) (Ref. 25), the spectrum deduced in Ref. 13 (Merdinger), the present results, two neutron-hole configurations (six different configurations), and two proton particle configurations (six different configurations).

mental 4^+ energy, indicating that the higher excitations are less collective and can be understood in terms of two-particle excitations.

For example, the 5^- state at 2276 keV can be suggested as a combination of the $(\nu h_{11/2}^{-1} \nu d_{3/2}^{-1})_{5^-}$ and the $(\nu h_{11/2}^{-1} \nu s_{1/2}^{-1})_{5^-}$ configurations. In the same way the 7_2^-, 8_1^-, and 9_1^- states at 3062, 3240, and 3455 keV, respec-

TABLE III. Summary of single-particle energies used in the shell-model calculations for ^{140}Nd.

Protons[a] (MeV)	Neutrons[b] (MeV)
$\pi d_{5/2}$: 0.0	$\nu d_{3/2}^{-1}$: 0.0
$\pi g_{7/2}$: 0.11	$\nu s_{1/2}^{-1}$: 0.19
$\pi h_{11/2}$: 0.82	$\nu h_{11/2}^{-1}$: 0.76
	$\nu d_{5/2}^{-1}$: 1.20
	$\nu g_{7/2}^{-1}$: 1.33

[a]Proton single-particle energies are given relative to the ground state of the ^{139}Pr nucleus (Ref. 23).

[b]Neutron single-hole energies are given relative to the ground state of the ^{141}Nd nucleus (Ref. 22).

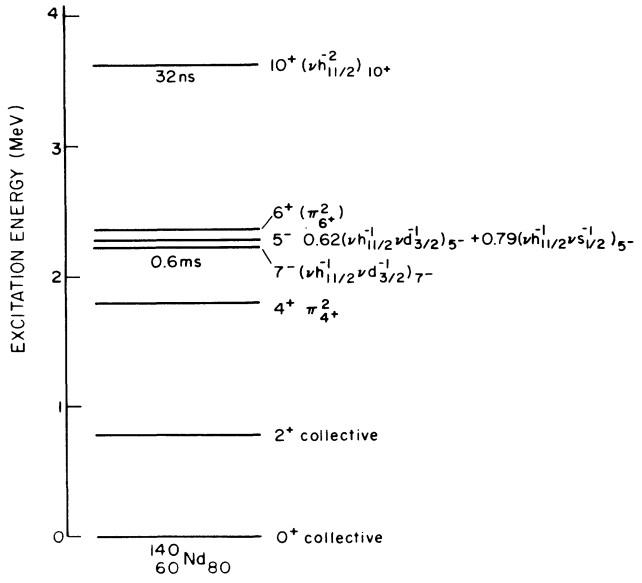

FIG. 7. Summary of the low-lying structure of ^{140}Nd.

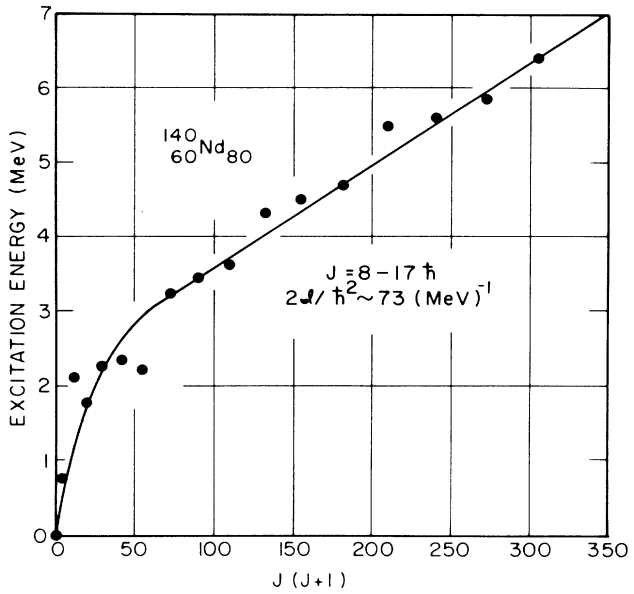

FIG. 8. Excitation energy versus $J(J+1)$ for ^{140}Nd.

tively, can be interpreted as two neutron-hole configurations:

$$7_2^-,\ (\nu h_{11/2}^{-1} \nu g_{7/2}^{-1})_{7^-} + (\nu h_{11/2}^{-1} \nu d_{5/2}^{-1})_{7^-}\ ;$$

$$8_1^-,\ (\nu h_{11/2}^{-1} \nu g_{7/2}^{-1})_{8^-} + (\nu h_{11/2}^{-1} \nu d_{5/2}^{-1})_{8^-}\ ;$$

$$9_1^-,\ (\nu h_{11/2}^{-1} \nu g_{7/2}^{-1})_{9^-}\ .$$

On the other hand, the lowest 6^+ states could be a combination of two proton states: predominantly $(\pi g_{7/2}^2)_{6^+}$ with some $(\pi g_{7/2} \pi d_{5/2})_{6^+}$. The 7^- and 10^+ states at 2222 and 3622 keV are already known to have two neutron-hole configurations, $(\nu h_{11/2}^{-1} \nu d_{3/2}^{-1})_{7^-}$ and $(\nu h_{11/2}^{-2})_{10^+}$, respectively. Although our suggestions on the configurational structure are based only on the excitation energy comparison, a diagonalization for the 5^- state at 2276 keV has been performed and the resulting component ratios are given in Fig. 7, which also summarizes our results for the low-lying states.

That deformation does not set in at higher angular momentum is illustrated in Fig. 8. For the higher excited states, the excitation energies follow a $J(J+1)$ dependence *on average*, but the average moment of inertia one extracts of $2\mathcal{J}/\hbar^2 \approx 73$ MeV^{-1} is close to the rigid sphere value. Therefore, the angular momentum arises from the alignment of the single particles and not collective rotation.

V. SUMMARY

We have measured the γ-ray deexcitation of states in ^{140}Nd up to $J=17$ and an excitation energy of 6411 keV. The structure of the low-lying levels of ^{140}Nd is dominated by two-neutron-hole configurations. Below the $Z=64$ shell gap, the 7^- and 10^+ isomers in the $N=80$ nuclei are predominantly two neutron-hole states, namely $(\nu d_{3/2}^{-1} \nu h_{11/2}^{-1})_{7^-}$ and $(\nu h_{11/2}^{-2})_{10^+}$, respectively, a conclusion supported by the $N=80$ systematics and g factor measurement.[19] There is no evidence for a change in structure from a predominantly single particle to deformed collective as a function of angular momentum. We shall investigate the effects of an extra proton outside of the ^{140}Nd core in a forthcoming paper by studying the deexcitation scheme of ^{141}Pm populated in the ^{126}Te(^{19}F,4n) reaction.

ACKNOWLEDGMENT

This work was supported by the U.S. Department of Energy through Contract No. DE-AC02-76ER03074.

*Present address: Department of Physics, University of California at Los Angeles, Los Angeles, CA 90024.
†Present address: Department of Physics, Rutgers University, New Brunswick, NJ 08903.

[1]G. A. Leander and P. Möller, Phys. Lett. **110B**, 17 (1982).
[2]J. L. S. Carvalho *et al.*, Phys. Rev. C **31**, 1049 (1985).
[3]P. J. Nolan *et al.*, Phys. Lett. **108B**, 269 (1982).
[4]P. J. Nolan, R. Aryaeinejad, A. H. Nelson, D. J. G. Love, D. M. Todd, and P. J. Twin, Phys. Lett. **128B**, 285 (1983).
[5]P. J. Nolan, A. Kirwan, D. J. G. Love, A. H. Nelson, D. J. Unwin, and P. J. Twin, J. Phys. G **11**, L17 (1985).
[6]A. Zemel, C. Broude, E. Dafni, A. Gelberg, M. B. Goldberg, J. Gerber, G. J. Kumbartzki, and K. H. Speidel, Nucl. Phys. **A383**, 165 (1982).
[7]M. Muller-Veggian, Y. Gono, R. M. Lieder, A. Neskakis, and C. Mayer-Böricke, Nucl. Phys. **A304**, 1 (1978).
[8]Yu V. Sergeenkov and V. M. Sigalov, Nucl. Data Sheets **34**, 475 (1981).
[9]B. J. Varley, R. Moscrop, S. Babkair, C. J. Lister, W. Gelletly, and H. G. Price, in *Capture Gamma-Ray Spectroscopy and Related Topics (Holiday Inn–World's Fair, Knoxville, Tennessee)*, proceedings of the 5th International Conference, AIP Conf. Proc. No. 125 edited by S. Raman (AIP, New York, 1984), p. 709.
[10]L. Ying, D. J. G. Love, A. Kirwan, A. H. Nelson, P. J. Nolan, and D. J. Unwin, Daresbury Report Vol. 23, p. 51, 1984.
[11]C. J. Lister *et al.*, Phys. Rev. Lett. **55**, 810 (1985).
[12]J. Ludziejewski and H. Arnold, Z. Phys. A **277**, 357 (1976).
[13]J. C. Merdinger, Phys. Scr. **24**, 249 (1981).
[14]E. Gülmez, M. W. Drigert, and J. A. Cizewski, Bull. Am. Phys. Soc. **31**, 836 (1986).
[15]E. Gülmez, H. Li, and J. A. Cizewski, Bull. Am. Phys. Soc. **30**, 1264 (1985).
[16]E. Gülmez, Ph.D. thesis, Yale University, 1986 (unpublished).
[17]L. K. Peker, Nucl. Data Sheets **26**, 473 (1979).
[18]E. K. Warburton, J. W. Olness, C. J. Lister, R. W. Zürmuhle, and J. A. Becker, Phys. Rev. C **31**, 1184 (1985).
[19]J. C. Merdinger, F. A. Beck, E. Bozek, T. Byrski, C. Gehringer, Y. Schutz, and J. P. Vivien, Nucl. Phys. **A346**, 281

(1980).
[20]R. D. Lawson, *Theory of the Nuclear Shell Model* (Oxford University, Oxford, 1980).
[21]P. W. M. Glaudemans, B. H. Wildenthal, and J. B. McGrory, Phys. Lett. **21**, 427 (1966); P. W. M. Glaudemans, P. J. Brussard, and B. H. Wildenthal, Nucl. Phys. **A102**, 593 (1967).
[22]R. K. Jolly and E. Kashy, Phys. Rev. C **4**, 887 (1971); S. El-Kazzaz, J. R. Lien, G. Lovhoiden, P. Kleinheinz, C. Ellegard, J. Bjerregaard, P. Knudsen, and J. Rekstad, Nucl. Phys. **A280**, 1 (1977).
[23]Wm. C. McHarris, D. B. Beery, and W. H. Kelly, Phys. Rev. Lett. **22**, 1191 (1969).
[24]T. Ishimatsu, H. Ohmura, T. Awaya, T. Nakagawa, H. Orihara, and K. Yagi, J. Phys. Soc. Jpn. **28**, 291 (1970).
[25]L. K. Peker, Nucl. Data Sheets **28**, 267 (1979).
[26]L. K. Peker, Nucl. Data Sheets **36**, 289 (1982).
[27]L. K. Peker, Nucl. Data Sheets **43**, 579 (1984).
[28]L. K. Peker, Nucl. Data Sheets **41**, 195 (1984).
[29]L. K. Peker, Nucl. Data Sheets **42**, 111 (1984).
[30]J. K. Tuli, Nucl. Data Sheets **27**, 97 (1979).